Influence of Machining Surface Finishing on Cavitation Resistance of a GWAW Deposited Cobalt Austenitic Stainless-Steel Coating

Mauricio Daniel Marczal
Henrique Ajuz Holzmann (haholzmann@utfpr.edu.br)
UTFPR: Universidade Tecnologica Federal do Parana https://orcid.org/0000-0001-5322-3791
Anderson Geraldo Marenda Pukasiewicz
Aldo Braghini Junior

Research Article

Keywords: Cavitation, erosion, roughness, machining, surface finish

Posted Date: April 8th, 2022

DOI: https://doi.org/10.21203/rs.3.rs-1514628/v1

Abstract

The cavitation phenomenon represents a serious efficiency problem for hydro generators. Long repair periods associated with a total equipment stoppage have a significant impact on the effective cost of turbine maintenance. Welding is followed by grinding finish, and depends on the operator's skill, which can cause significant changes in the profile of the component, as well as in its roughness. Low values of roughness in the recovered surface can reduce the loss of mass by cavitation. Understanding the cavitation phenomenon, associated with the surfaces obtained by different machining conditions, can promote a better understanding of wear mechanisms related to cavitation on machined surfaces. This article has evaluated the mass loss and the roughness profiles produced by different conditions of machining in a cavitation resistant austenitic stainless-steel coating, deposited on to martensitic stainless steel. Polished and ground samples were used as surface condition references. The results indicated that the surface finish obtained by machining influences the cavitation process, mostly in the incubation stage. The cavitation mass loss occurs mainly through pitting mechanisms in micro-burr regions with detachment of adhered material, resulting from machining conditions. As for the evolution of the roughness throughout the experiments, the polished, ground and machined samples showed different behaviors.

1. Introduction

Cavitation is a phenomenon in which bubbles are generated in a fluid. The formation of the bubbles occurs due to a reduction of pressure at a certain point in the fluid, followed by a collapse in a high-pressure region as described by Zhang et al. [1]. The collapse of the bubbles creates shock waves, forming highly destructive microjets that reach extremely high pressures, of GPa order, as found by Okada et al. [2]. Such impact pressures cause a fatigue of the material, leading to the propagation of cracks and severe material degradation. The repetitive occurrence of the phenomenon initiates a process of nucleation of microcracks, generating a process of damage on the material surface. Elements such as pump rotors and turbine blades are examples of components that are susceptible to the cavitation phenomenon.

To minimize the cavitation mass loss on hydraulic components, some austenitic alloys with cobalt content were develop as coating, which have a high mechanical strength and energy absorption. The cavitation resistance of these austenitic steels is promoted through the material's ability to absorb impact, through a structural phase transformation from austenite γ to martensite α' and/or martensite ε, due to its low stacking-fault energy as noted by Ribeiro et al. [3] in his research. This phase transformation generates a high energy absorption. Still considering phase transformation as a means of absorbing energy, Krella and Czyzniewski [4] found in their research that this energy is absorbed by changes in dislocation structure, some of it used by the phase transformation $Fe\gamma \rightarrow Fe\alpha$ + carbide in metastable austenitic steels as noted by Wu et al. [5].

Scratches and high roughness, mentioned by Hao et al. [6], high porosity, mentioned by Taillon et al. [7] and cracks reduce material strength and lead to accelerated material loss. The surface finish is correlated with the roughness, which can be associated with different cavitation stages. Different roughness parameters can be used for the study of cavitation phenomenon, as well as maximum profile height (Rz) and the total roughness (Rt) standing out for their higher sensitivity, as observed by Ahmed et al. [8].

Usually, different arc welding processes are used to deposit cobalt stainless- steel alloys. After deposition, grinding is performed to ensure appropriate profile and roughness to the welded surface. In this process of surface finishing, the cavitation resistance of the alloy is directly affected by the generation of high levels of surface roughness. This behavior could be observed by Chiu et al. [9] when these researchers evaluated the evolution of surface roughness of three metallic materials (316L stainless steel, CP titanium, and brass) and by Lin at el. [10] when they observed the cavitation erosion behaviors of FeNiCrBSiNbW coatings with different surface roughness levels. Da Cruz et al. [11] also observed that the strain influences cavitation resistance. Machining processes such as milling allow for better results in terms of final roughness and strain induced processing.

The aim of this research is to evaluate the influence of machining on the cavitation resistance of a cobalt austenitic stainless alloy, deposited by gas metal arc welding process, under different machining conditions. Two types of Ball Nose end mills were used, varying feed rate and cutting speed, the performance of the tools in the new and worn state were also compared.

2. Methodology

In this section, the materials, equipment and procedures used in this research are presented in an integrated manner.

2.1 Materials

The materials used were martensitic stainless steel ASTM A743-CA6NM as a substrate, where two layers of austenitic stainless steel with cobalt were deposited by arc welding process. These materials are typically used by manufactures, and also for the maintenance of hydraulic components. The chemical composition was performed by energy dispersion spectroscopy (EDS) Oxford x-Act (Oxford Instruments, Abingdon, United Kingdom) in a scanning electron microscope (SEM) type Tescan Mira 3 model (Tescan, Brno, Czech Republic), and presented in Table 1.

Table 1
Chemical composition of the coating deposited by welding *

	Si	Mn	Cr	Ni	Co	Cu	Mo
Co stainless steel	2.9%	8.34%	16.26%	0.12%	10.9%	0.1%	-
ASTM A743-CA6NM	0.8%	0.9%	14.09%	3.8%	-	-	0.9%
* Carbon, Nitrogen, Phosphorus and Sulfur were not measured by EDS							

2.2 Sample Preparation

For deposition of the coating on the substrate GMAW (Gas Metal Arc Welding) process was used in a welding equipment ESAB Smashweld 315 model (ESAB, Gothenburg, Sweden). All depositions were conducted on a ASTM A743-CA6NM base substrate and sectioned with dimensions of 15 mm x 25 mm x 25 mm. A total of 2 weld bead were performed (overlap). A speed control guide IMC Tartílope V1 (IMC, Florianopolis, Brazil) was used to assist the deposition, and temperature control by thermocouple was performed in each pass. The parameters used for welding are described in Table 2.

Table 2
Welding deposition parameters

Parameters	
Wire diameter	1.2 mm
Process	GMAW
Tension	22 V
Wire feed speed	1.5 m/min
Number of weld bead	2
Direction	Flat
Welding speed	0.25 m/min
Protetion gas type	Air – 2% O2
Protective gas flow	15 l/min
Interpass temperature	150°C

The deposited surface was subsequently rough milled to remove the ends of the weld bead reinforcements.

The surface finishing process was carried out by milling in a Hermle machining center, model C800 U (Hermle, Gosheim, Germany), using ball nose end mills with a diameter of 12 mm, being: a mill with an interchangeable insert with 2 cutting edges (manufacturer code R216F-1230 EL 1010) and an

interchangeable head cutter with 4 cutting edges (manufacturer code 316-12BM440-12060G 1030). The cutters were used to generate the surfaces in two different cutting edges sharpening conditions: new (sharp edge as supplied by the manufacturer) and worn (after 0.2 mm maximum flank wear was obtained), the tools used are shown in Fig. 1.

The studied cutting parameters were cutting speed (vc) and the feed per tooth (fz). The radial depth of cut (ae) was set at 0.1 mm and the axial depth of cut (ap) at 0.5 mm. Each sample received a coding for analysis (First column of Table 3). The parameters used are presented in Table 3.

Table 3
Experiment conditions

Condition	Cutting edge	Mill	f_z (mm/tooth)	v_c (m/min)
1W	*Worn*	Interchangeable Insert	0.1	200
2W		Interchangeable Head	0.1	200
3W		Interchangeable Insert	0.1	300
4W		Interchangeable Head	0.1	300
5W		Interchangeable Insert	0.08	200
6W		Interchangeable Head	0.08	200
1N	*New*	Interchangeable Insert	0.1	200
2N		Interchangeable Head	0.1	200
3N		Interchangeable Insert	0.1	300
4N		Interchangeable Head	0.1	300
5N		Interchangeable Insert	0.08	200
6N		Interchangeable Head	0.08	200

Two samples were prepared for comparison with machined samples, one polished and the other ground. The polished sample was produced by sequential grinding of water sandpaper of 220, 360, 600, and 1200 mesh granulometry, followed by polishing with diamond slurry of 1 µm and 0.25 µm. The ground sample was made by manual angle grinding using a 4.5" disc with 120 mesh.

2.3 Cavitation Test

The accelerated cavitation test was performed following the ASTM G32 [12] standard modified for the indirect method on Qsonica Q700 equipment (Qsonica, Newtown, USA). Deionized water was used, at a controlled temperature of 25°C with the samples immersed at a depth of 20 mm. The distance between the sonotrode tip and the sample was calibrated at 500 µm. The vibration frequency of the system was set to 20 kHz, the sonotrode diameter was 19 mm. The total test time was set at 20 hours for each

sample, with 2 hours intervals for the sample to be cleaned, in acetone of analytical purity in ultrasonic bath, drying with hot air blast and subsequent weighing on a precision balance Shimadzu AUX 220, with a resolution 0.1 mg.

2.4 Optical Profilometry

The samples were submitted to optical profilometry, in a Taylor Hobson CCI Lite profilometer (Taylor Hobson, Leicester, United Kingdom), using 10x lens, and the data were processed by the Talymap Gold 6.2 software (Taylor Hobson, Leicester, United Kingdom), to obtain the parameter of maximum average surface height (Sz) in the cavitated region. The analysis area was 1.67 mm x 1.67 mm with the sample always oriented at the same initial measurement position. Data was collected every 2 hours of cavitation test.

2.5 Scanning Electron Microscopy

Images of the samples' surfaces were acquired by means of a Tescan Vega 3 (Tescan, Brno, Czech Republic) scanning electron microscope, operated at 20 kV, to obtain the topographic aspect of the cavitated surface. The erosion mechanisms during the cavitation process were determined by analyzing the SEM micrographs of the cavitated surfaces regions.

2.6 Hardness Test

The hardness of the samples, before and after cavitation tests, was evaluated with a Shimadzu HMV-G20 microdurometer equipment (Shimadzu Corporation, Kyoto, Japan), Vickers scale, with a load of 300 gf for 15 seconds. Fifteen measurements were performed at intervals of 0.4 mm to obtain the hardness of the material.

3. Results And Discussion

3.1 Surface Profile Analysis Before Cavitation Tests

The type and condition (new or worn) of the tool changed the initial morphology of the machined surfaces. Figure 2 shows the images obtained by SEM of the surfaces machined before cavitation, produced by interchangeable insert tool in new condition (A) and worn (B) for cutting parameter set at fz 0.1 mm/ tooth and vc 200 m/min. The topographic differences resulting from machining with the new tool and the worn tool can be observed.

The new tool has a more significant shear effect on the machined surface, while the worn tool generates a more pronounced mechanical forming. This generates crushing and leaves portions of residual chips, due to cold welding on the surface. The cutting edge at the center of the tool does not promote a perfect shear in this region, causing a portion of the material to be crushed and pushed out of the center of the tool, not being removed by the next cutting edge. Even though the appearance and material removal mechanism for the two different tool conditions are not similar, the initial Sz roughness has a very similar level, with 6.12 µm for new tool (condition 1N) and 5.46 µm for the worn tool (condition 1W). Although

topographically different, the surfaces have a similar roughness. The initial roughness of the samples is shown in Table 4.

Table 4
Initial SZ roughness of the samples used in the tests

Initial S_Z roughness (µm)								
Condition	1N	2N	3N	4N	5N	6N	**Grinded**	**Polished**
S_Z roughness (µm)	6.12	4.84	6.07	5.04	6.48	4.96	9.95	0.18
Condition	1W	2W	3W	4W	5W	6W		
S_Z roughness (µm)	5.46	8.66	5.64	5.01	5.03	14.74		

Most machined samples showed similar behavior in terms of roughness. The reduction on the feed per tooth impacts even more strongly on the machining result compared to the cutting speed for the worn interchangeable head tool. The aspect of the surface produced by the interchangeable head tool can be observed on the Fig. 3, under lower feed rate conditions (fz 0.08 mm/tooth) and lower cutting speed (vc 200 m/min). The result of forming with the worn tool is even more intense (Fig. 3B (6W) compared to Fig. 3A (6N)). Larger plates of adhered material can be observed, typical trails of the cutting tool (Fig. 3B) are not observed in the same intensity in the new tool (Fig. 3A).

3.2 Cavitation Resistance of the Different Surfaces Conditions

The Fig. 4 shows the mass loss accumulated during the test for samples machined with new tools. The process of cavitation erosion, in the machined samples, in the first hours of the test is very different when compared to the polished reference sample. The results obtained in terms of time and accumulated mass loss when compared to the unpolished samples were similar to the results found by Da Cruz et al. [11].

The higher mass loss in the initial hours of the test, combined with the observation of the worn surfaces, show that most of the material that eroded at the beginning of the test was due to the removal of micro-burrs resulting from the machining process. These burr zones are preferred pullout zones. In Fig. 5 the appearance of sample 4N can be observed: (A) without cavitation, indicating material plates adhered to the surface, and (B) after 6 hours of testing, showing the burrs as the main material removal zone. These burrs undergo an extensive process of hardening and lose the ability to absorb energy, thus suffering a fragile [11].

There are small occurrences of pit formations, suggesting that the main mechanism until the sixth hour of testing was in fact the loss of adhered material associated with the pullout of small portions of material in the micro-burrs. This pullout is due to fatigue fracture induced by the collapse of the bubbles on the surface, because when the pressures exceed the elastic limit of the material it ends up suffering plastic deformation until a microscopic failure occurs.

Figure 6 shows the mass loss accumulated during the test for samples machined with worn tools. The mass loss occurs early and immediately after two hours of testing for all samples. The behavior is relatively similar to that of surfaces machined by new tools, however it differs in the rate of mass loss and also in the accumulated total values.

The mass loss curves of the samples machined by the worn tool indicate a higher loss of mass at the beginning of the cavitation tests and a lower rate of mass loss after the initial period of mass loss (similar to the incubation period observed in the polished sample), which is in accordance with what was observed by Da Cruz et al. [11]. Similarly, to the samples machined by the new tool, the mass loss mechanism also occurred with the pulling of material through the microfracture by fatigue.

In Fig. 7 it is possible to observe the surface of the 4W sample in: (A) 6 hours of cavitation, showing the removal of micro-burrs and in (B) after 20 hours of cavitation, the presence of pitting regions, as well as greater depth of the pits formed. Krella et al. [13] in their research on cavitation erosion, also found pits during the cavitation process, in the grain boundaries preference location.

Samples originating from machined surfaces, with the largest amount of mass lost at the end of the test, were mostly those that showed the greatest degradation of the initial surface.

In this way a similar behavior can be verified among the machined samples (new and worn tools) and the grinded sample, regarding the increase of the mass loss curve, and diverging from the polished sample. In the polished sample an incubation period of up to approximately 10 hours of testing is observed. After the incubation period, there is an increase in the rate of mass loss, associated with the acceleration period of the cavitation process, according to Iwai et al. [14]. A great part of this characteristic is due to the form of preparing the surface of the samples, because during the grinding and machining process, especially with worn tools, a considerable plastic deformation of the material occurs. This plastic deformation is associated with great efforts to remove material, and consequently an insertion of energy in the material surface, and thus a localized phase transformation may occur. As less effort is applied during the polishing of the sample, this transformation may be minimal, resulting in a characteristic incubation period. Krella and Czyzniewski [4] also found in their research that the phase transformation influences the behavior of mass loss.

3.3 Roughness Evolution During Cavitation Tests

The roughness assessment is a very useful tool to analyze the effect of cavitation over time, as observed by Ahmed et al. [8]. Krella et al. [13] considering the Ra and Ry parameter in your research to monitor the evolution of cavitation. The roughness evolution curves for the machined samples had a subtle drop behavior from the maximum height of the profile in the initial hours of the test, observing the phenomenon in the surfaces generated with new and worn geometry. This occurrence is cited by Chiu et al. [8]. The curves of roughness evolution, shown in Fig. 8, for the machined samples with new tool conditions, show that the effect is more discrete, being little affected with the change in the cutting parameters of the interchangeable insert tool.

In the interchangeable head tool, the parameters are more significant, and it was found that the increase in cutting speed promoted a more accentuated elevation in the level of roughness, while the reduction in the feed per tooth reduced the roughness growth rate throughout the test.

When observing the roughness curves of the samples machined by the tool with worn cutting geometry in Fig. 9, it is noted that the two cutters also present different behaviors comparing the conditions 1W with 2W and 5W with 6W. However, this different behavior is observed in 3W and 4W.

The interchangeable insert tool (new and worn) had similar evolution in all cutting conditions and no changes were observed in the evolution of the profile that would indicate influence of either the cutting speed or the feed per tooth. As for the interchangeable head cutter, the opposite influence with the new geometry is clearly noted. The lower feed in addition to promoting higher initial roughness, also modified the curve evolution profile, with a drop in the first six hours, growing until the tenth hour and stabilizing its growth rate until the end of the test. The influence of the feed is therefore more significant as also found by Gökkaya and Nalbant [15]. This behavior is related to the extraction of adhered material plates, which as a result of the large number of scales, initially reduced the roughness of the sample, revealing the base portion of the material, which was more affected by the microfractures.

In Fig. 10, in the sample 6W (machined by interchangeable head tool), the detachment of the layers of scales adhered in the sixth hour of test is observed (A). In Fig. 10 (B) a topographic change caused by revealing the base portion of the adhered layer, with consequent increase in roughness, in the tenth hour is observed. In this same sample (Fig. 10 (B)) the greatest initial roughness is correlated with the greatest loss of mass. According to Tzanakis et al. [16] the surface roughness increased, accelerating the erosion rate of the materials and Lin et al. [10] also found in their research that the increase of initial surface roughness of the material tested showed an increase in mass loss of cavitation erosion damage.

In Fig. 8 and Fig. 9, it is possible to identify similar finish characteristics in the surfaces of the samples obtained by machining with a small increase of value in roughness within 20 hours of test. As for the ground and polished samples, there is a great increase in the roughness values, requiring the insertion of a break in the graphs, in order to represent the curves during the cavitation process. Thus, it is possible to see three distinct groups of behavior regarding roughness, being compatible with polished, ground and machined samples.

The polished sample tends to have a better initial surface finish when compared to other samples, and it remains with some small variations until close to 10 hours of cavitation test and from this moment presents an increase in the values of roughness, being associated with the transition from the incubation period to the acceleration period and a higher rate of mass loss.

The ground sample starts with a higher roughness than the others, and follows almost linear profile of elevation in values of roughness until 10 hours of test, followed by an exponential growth. The machined samples show a linear growth from the beginning to the end of the test, 20 hours. This behavior from the

point of view of process control is extremely important, since its roughness can be more accurately estimated, thus being possible to perform preventive maintenance without abrupt material failures.

The roughness of the samples could be correlated with their loss of mass, as this is a way of monitoring the cavitation stages as also noted by Ahmed et al. [8]. In the cases of the ground and polished surface there is an expectation of a great worsening of the surface, culminating in an increase in the rate of mass loss, for extrapolation of the cavitation test in more than 20 hours.

3.4 Surface Profile Analysis After Cavitation Tests

In all machining conditions, the final topography shows material removal effects associated with ductile microfracture, alternating between pulling out micro-burrs and pitting nucleation.

Typical triangular structures of hardening and phase transformation were not observed in the material, as presented by Xiaojun et al. [17] who studied the cavitation process of the same coating material used in this research. There was no evidence for any case of machined sample, only occurring in the polished sample. This fact may be associated with the induced stress in the material caused by the machining work. The effect in the acceleration stage, however, slows down mass loss when compared to the machined sample, as can be seen in the topographies at the end of the test. A partial preservation of the machined surface can be observed, which did not occur with the ground sample. This demonstrates that the wearing mechanism for the 3 conditions (polished, ground and machined surface) is different and varies according to the stage in which the cavitation effect is found. The surface topographies at the end of the test for the machined samples are shown in Fig. 11.

The surface topography of the reference samples, after 20 hours of testing, did not show significant preservation of its original aspect. The evolution of the ground sample followed the same mechanism of the machined samples, but was much more accelerated, and in 14 hours presented a much more eroded aspect than in all machined samples. Figure 12 (A, B, C, D) show a ground surface and the evolution of its wear up to 20 hours of cavitation tests and Fig. 12 (E, F) represent surfaces machined with 14 hours of testing, presenting less damage to the sample and preserving its original appearance (Compare Fig. 12C with Fig. 12E and 12F).

The polished reference sample, Fig. 13, shows an abrupt change in the surface between the 10th and 20th hour of test. Its accelerated mass loss culminated in almost total surface change after the 20 hours test. For polished samples Park et al. [18] indicates the transformation of phases during the cavitation process and Tzanakis et al. [16]. The increase in the mass loss with the increase in the roughness of the surface.

As for the variation of the machining parameters, it was not possible to obtain a clear distinction between the samples. It was possible to identify the link between the samples' surfaces produced by the interchangeable insert tool and another interchangeable head cutter, not interfering if they were new or worn. The exception was the 6W sample, which presented the greatest roughness and the greatest loss of mass due to cavitation, which is due to its greater flank wear.

Observing the results obtained, a clear distinction can be seen between the polished, machined and grinded samples, which can exalt the lowest level of roughness in the machined samples during the course of the cavitation test. It is expected that with more than 20 hours of cavitation test, the polished samples and grinders will produce more and more rough surfaces and consequently present a greater loss of mass.

This study helps to identify greater predictability as to the roughness and loss of mass in the machined samples, favoring the control of the process and reducing the need to maintain surfaces subject to cavitation.

3.5 Hardness Evolution Before and After Cavitation Tests

The Vickers average hardness profile before and after the cavitation is observed in Fig. 14. It is observed that the machined samples showed a great dispersion of results, indicating different levels of hardening and consequently mechanical work. Only samples 3 and 6 (non-cavitated samples) showed some hardness difference in the comparison between the test with a new and worn tool.

As expected, the polished sample had the lowest hardness before the cavitation test, while the ground, 6N and samples 1N and 1W had the highest initial hardness. In general, there was no tendency for greater or lesser loss of initial mass with samples of higher initial hardness.

It should be analyzed in these samples that the effects of burr formation in the machining process interfere significantly with the loss of mass process, as well as with the mechanical work effect of loss of mass, thus making it difficult to correlate the results.

With the analysis of Vickers microhardness, performed after the cavitation tests, it can be observed that there was an increase in the hardness in the region after the cavitation test in all tested samples, which is compatible with what was found by Zhou et al. [19]. The increase in hardness after cavitation tests demonstrates hardening induced by material of deposition phase transformation, a mechanism by which it presents a high resistance to cavitation, as observed by Li et al. [20] in his research. Although all the samples showed hardening, there is no relation regarding the initial measured hardness and resistance to cavitation, whereas all samples had very similar levels in the final hardness values.

4. Conclusions

From the results obtained, this article contributes to clarify the influence of surface finish on cobalt austenitic steel alloy, when submitted to the cavitation process.

As for the machining of the samples, a differentiation can be seen between the results produced by the interchangeable insert tool and those with interchangeable head, so the type of tool is more important than its condition (new or worn) within the same maximum wear limits of the tool.

The wear mechanism occurred on the surfaces involves the fatigue process, started mainly in burr regions or rough tracks that occurred during machining, followed by the formation of pits formed by the mechanical action of the implosion of the bubbles, which do not have a preferred region to emerge.

The type of wear mechanism is influenced by the presence of material crushing on the machined surface. The smaller the portion of crushed/adhered material, the higher is the tendency for pitting formations. The greater the portion of crushed/adhered material, the more intense is the presence of burr fracture.

It is noticeable that the machining favored a stable increase in roughness as the loss of mass occurred during cavitation, thus these samples have greater predictability, favoring the application of this technique in the preparation of the surface subject to cavitation.

No correlation was found between the initial hardness of the samples and the loss of mass.

Declarations

Funding

The authors did not receive support from any organization for the submitted work.

Conflicts of interest/Competing interests

The authors declare that they have no conflict of interest.

Availability of data and material

Available on request.

Code availability

Not applicable

Authors' contributions

All authors contributed to the study conception and design. **Maurício Daniel Marczal:** Methodology, Validation, Investigation, Data curation, Writing – original draft. **Henrique Ajuz Holzmann:** Data curation, Methodology, Writing – original draft, Writing - review & editing. **Anderson G. M. Pukasiewicz:** Formal analysis, Writing - review & editing. **Aldo Braghini Junior:** Methodology, Supervision, Writing - review & editing, Visualization.

Ethics approval

Not applicable

Consent to participate

Not applicable

Consent for publication

Not applicable

References

1. Zhang X, Liu C, Liu X, Dong J, Yu B (2009) Cavitation erosion behavior of WC coatings on CrNiMo stainless steel by laser alloying. Int J Min Metall Mater 16(2):203–207. https://doi.org/10.1016/S1674-4799(09)60034-0
2. Okada T, Iwai Y, Awazu K (1989) A study of cavitation bubble pressures and erosion part 1: a method for measurement of collapse pressures. Wear 133(2):219–232. https://doi.org/10.1016/0043-1648(89)90037-9
3. Ribeiro HO, Buschinelli AJA, Dutra JC, D´Oliveira ASCM (2010) Resistência à erosão por cavitação de aços inoxidáveis austeníticos CrMnSiN depositados por PTA. Soldagem & Inspeção 15(2):121–129 (in Portuguese). https://doi.org/10.1590/S0104-92242010000200006
4. Krella A, Czyzniewski A (2007) Influence of the substrate hardness on the cavitation erosion resistance of TiN coating. Wear 263(1–6):395–401. https://doi.org/10.1016/j.wear.2007.02.003
5. Wu CZ, Chen YJ, Shih TS (2002) Phase transformation in austempered ductile iron by microjet impact. Mater Charact 48:43–54. https://doi.org/10.1016/S1044-5803(02)00232-2
6. Hao J, Zhang M, Huang X (2018) The influence of surface roughness on cloud cavitation flow around hydrofoils. Acta Mech Sin 34(1):10–21. https://doi.org/10.1007/s10409-017-0689-0
7. Taillon G, Pougoum F, Lavigne S, Ton-that L, Schulz R, Bousser E, Savoie S, Martinu L, Klemberg-sapieha J (2016) Cavitation Erosion Mechanisms in Stainless Steels and in Composite Metal – Ceramic HVOF Coatings. Wear 364–365:201–210. https://doi.org/10.1016/j.wear.2016.07.015
8. Ahmed SM, Hokkirigawa K, Oba R, Matsudaria Y (1990) Developing stages of ultrasonically produced cavitation erosion and corresponding surface roughness. JSME Int J Serie II 33(1):11–16. https://doi.org/10.1299/jsmeb1988.33.1_11
9. Chiu KY, Cheng FT, Man HC (2005) Evolution of surface roughness of some metallic materials in cavitation erosion. Ultrasonics 43(9):713–716. https://doi.org/10.1016/j.ultras.2005.03.009
10. Lin J, Wang Z, Cheng J, Kang M, Fu X, Hong S (2017) Effect of initial surface roughness on cavitation erosion resistance of arc-sprayed Fe-based amorphous/nanocrystalline coatings. Coatings 7(11):1–9. https://doi.org/10.3390/coatings7110200
11. Da Cruz JR, Henke SL, D'Oliveira ASCM (2016) Effect of cold work on cavitation resistance of an austenitic stainless-steel coating. Mater Res 19(5):1033–1041. https://doi.org/10.1590/1980-5373-MR-2015-0442
12. ASTM G32 (2016) N. Standard Test Method for Cavitation Erosion Using Vibratory Apparatus. ASTM International. Avaliable in: < www.astm.org &gt

13. Krella AK, Zakrzewska DE, Marchewicz A (2020) The resistance of S235JR steel to cavitation erosion. Wear 452–453:203295. https://doi.org/10.1016/j.wear.2020.203295
14. Iwai Y, Okada T, Tanaka S (1989) A study of cavitation bubble collapse pressures and erosion part 2: Estimation of erosion from the distribution of bubble collapse pressures. Wear 133(2):233–243. https://doi.org/10.1016/0043-1648(89)90038-0
15. Gökkaya H, Nalbant M (2006) The effects of cutting tool coating on the surface roughness of AISI 1015 steel depending on cutting parameters. Turk J Eng Environ Sci 30(5):307–316
16. Tzanakis I, Bolzoni L, Eskin D, Hadfield M (2017) Evaluation of cavitation erosion behavior of commercial steel grades used in the design of fluid machinery. Metall Mater Trans A 48(5):2193–2206. https://doi.org/10.1007/s11661-017-4004-2
17. Xiaojun Z, Procopiak LAJ, Souza NC, D'Oliveira ASCM (2003) Phase transformation during cavitation erosion of a Co stainless steel. Mater Sci Engineering: A 358(1–2):199–204. https://doi.org/10.1016/S0921-5093(03)00297-1
18. Park MC, Kim NK, Shin GS, Kim SJ (2012) Effects of strain induced martensitic transformation on the cavitation erosion resistance and incubation time of Fe – Cr – Ni – C alloys. Wear 274–275:28–33. https://doi.org/10.1016/j.wear.2011.08.011
19. Zhou Z, Fu W, Zhu Z, Li B, Shi Z, Sun S (2018) Excellent Mechanical Properties and Resistance to Cavitation Erosion for an Ultra-Low Carbon CrMnN Stainless Steel through Quenching and Partitioning Treatment. Int J Min Metall Mater 25(5):547–553. https://doi.org/10.1007/s12613-018-1601-z
20. Li C, Zhu R, Zhang X, Huang P, Wang X, Wang X (2020) Impact of surface ultrasonic rolling on cavitation erosion behavior of 304 stainless steel. Surf Coat Technol 383:125280. https://doi.org/10.1016/j.surfcoat.2019.125280

Figures

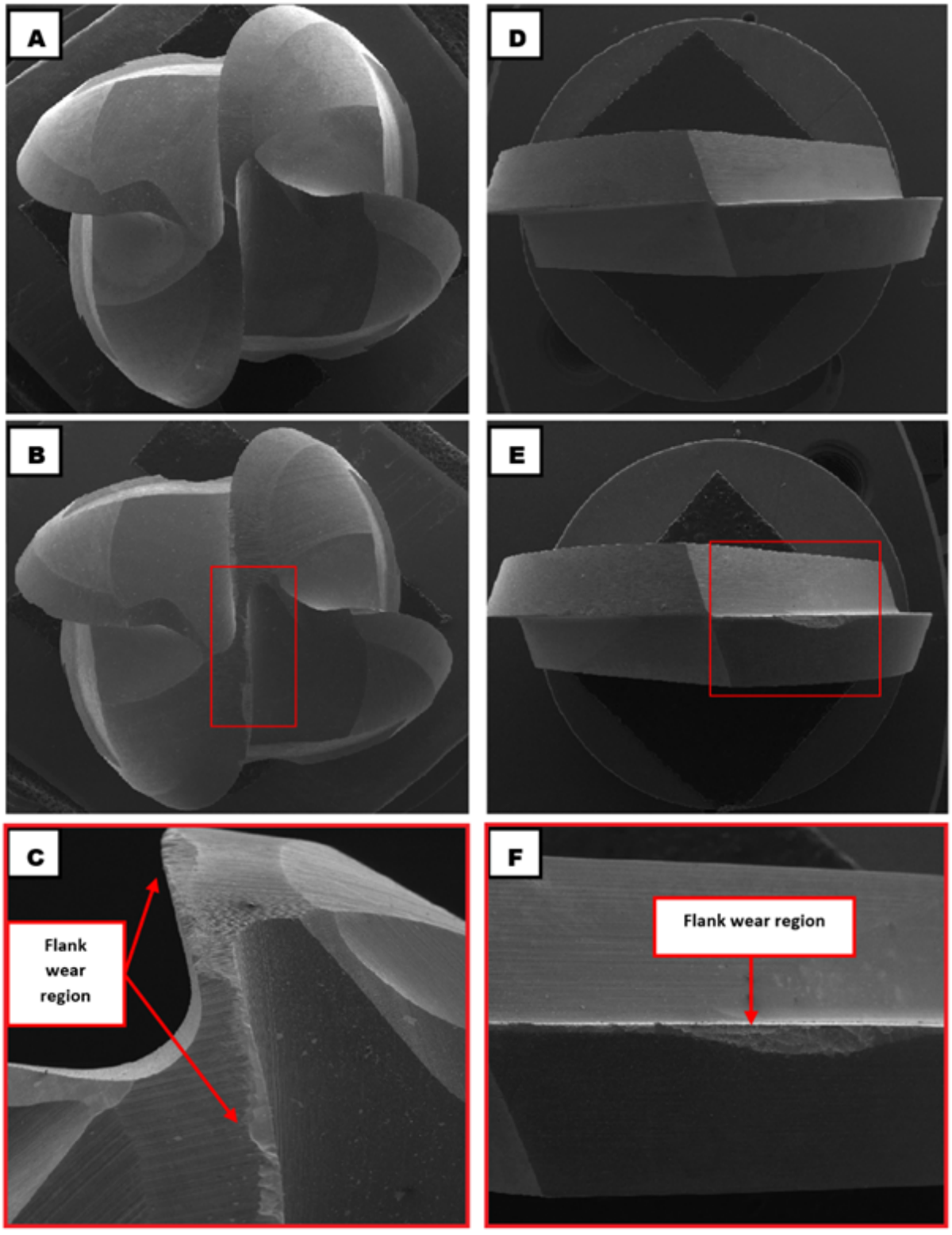

Figure 1

Images of the tools used in surface preparation - (A) interchangeable head new condition, (B) interchangeable head worn condition, (C) enlargement of the flank wear region of the worn interchangeable head tool, (D) interchangeable insert condition new, (E) insert worn condition and (F) enlargement of the flank wear region of the worn interchangeable insert tool

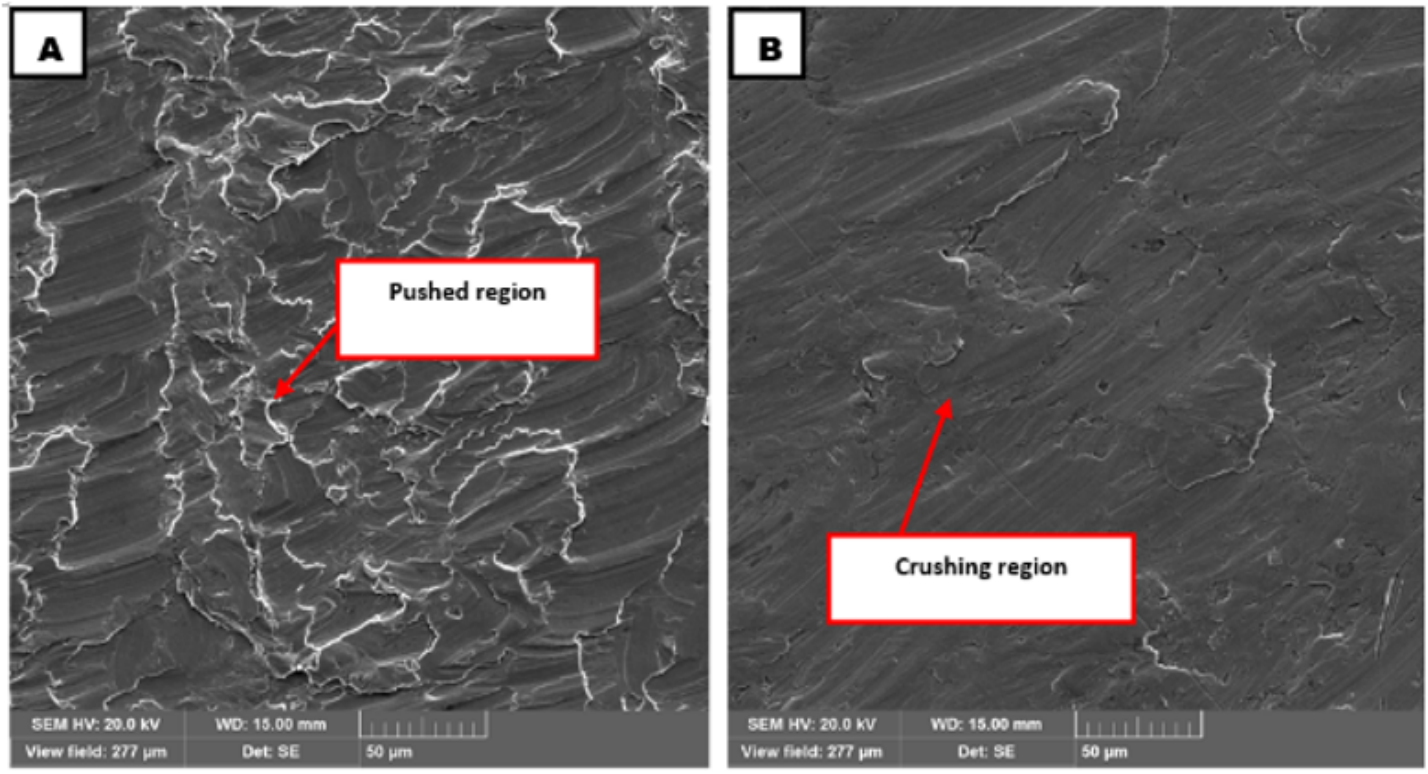

Figure 2

Surface topography in the initial condition of samples (A) 1N and (B) 1W

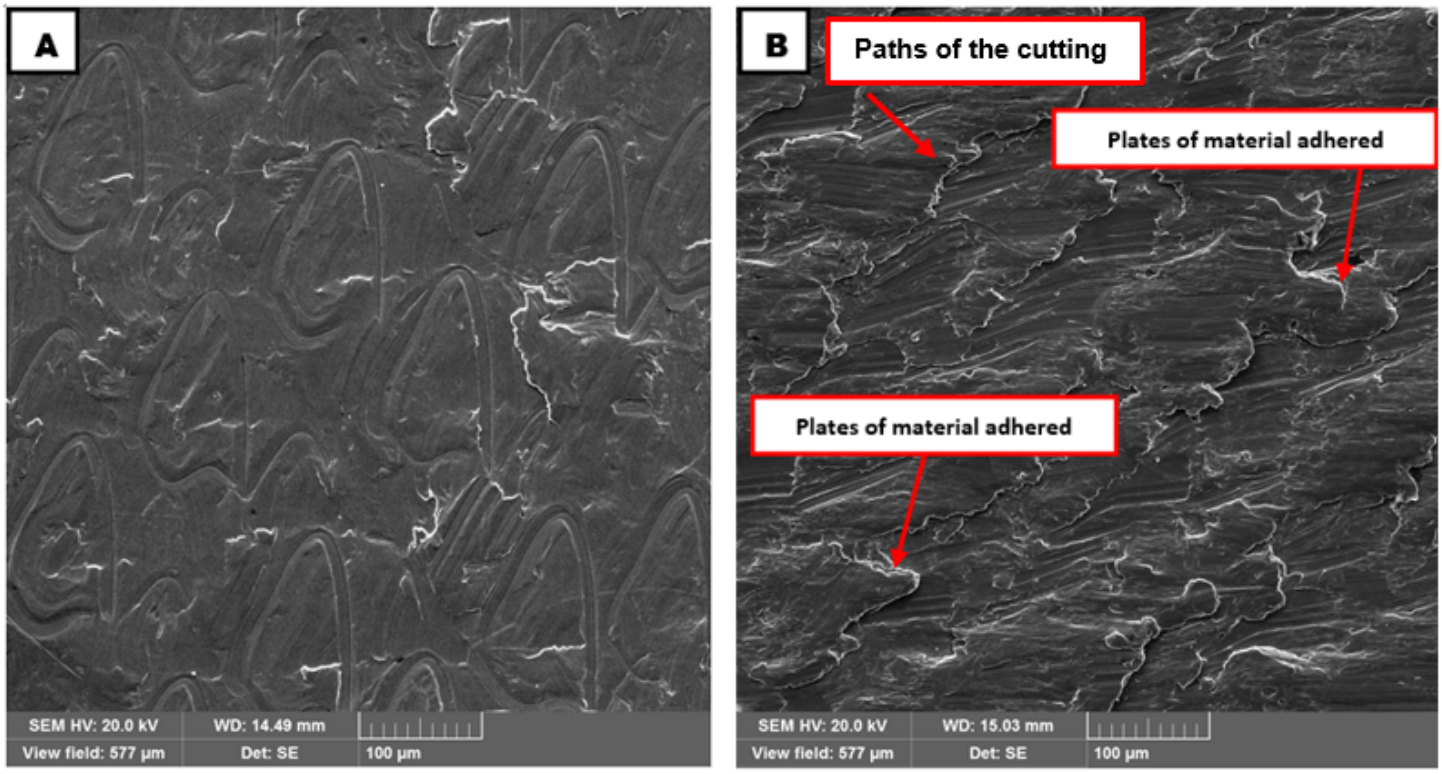

Figure 3

Surface morphology in the initial condition of samples (A) 6N and (B) 6W

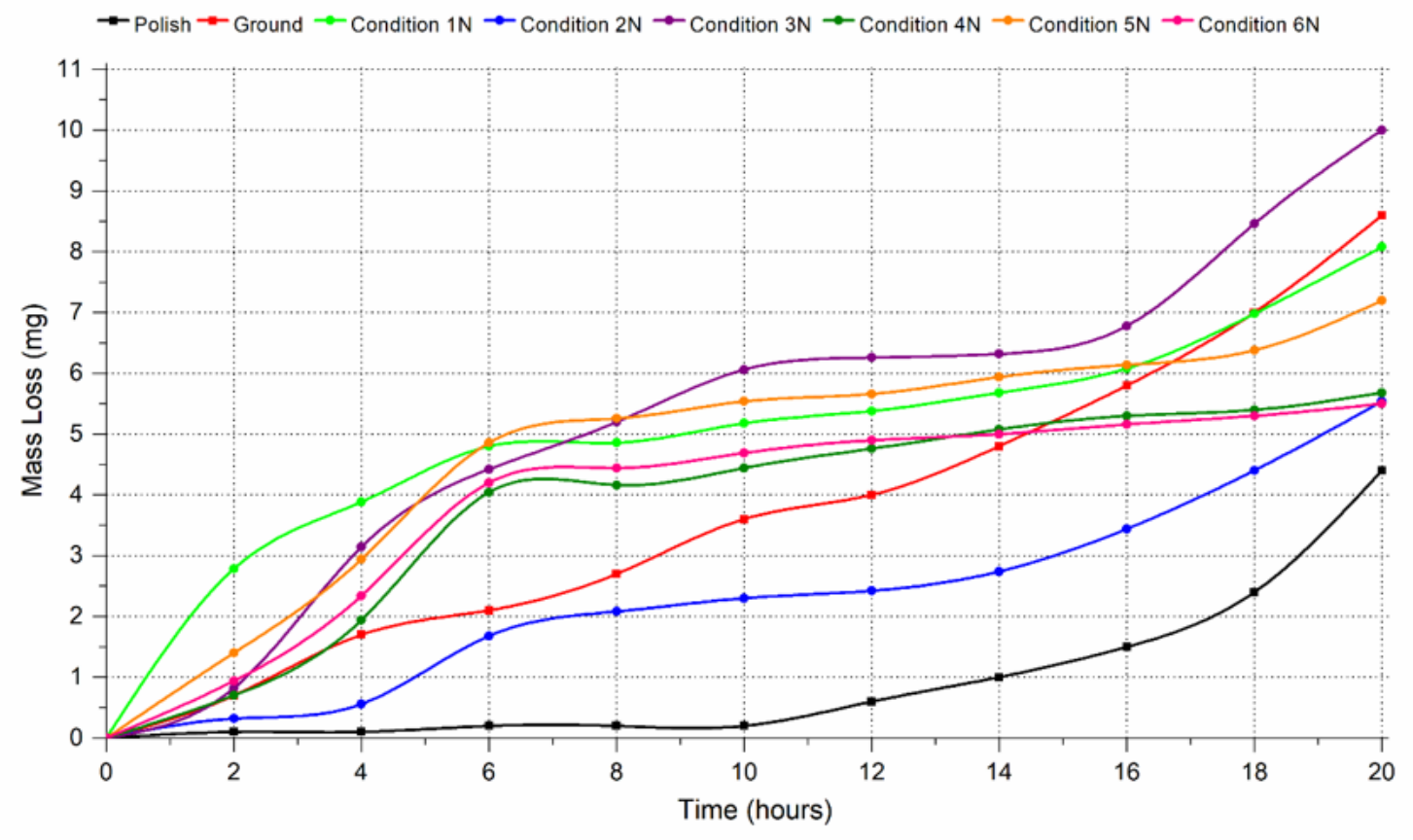

Figure 4

Accumulated mass loss – new tools

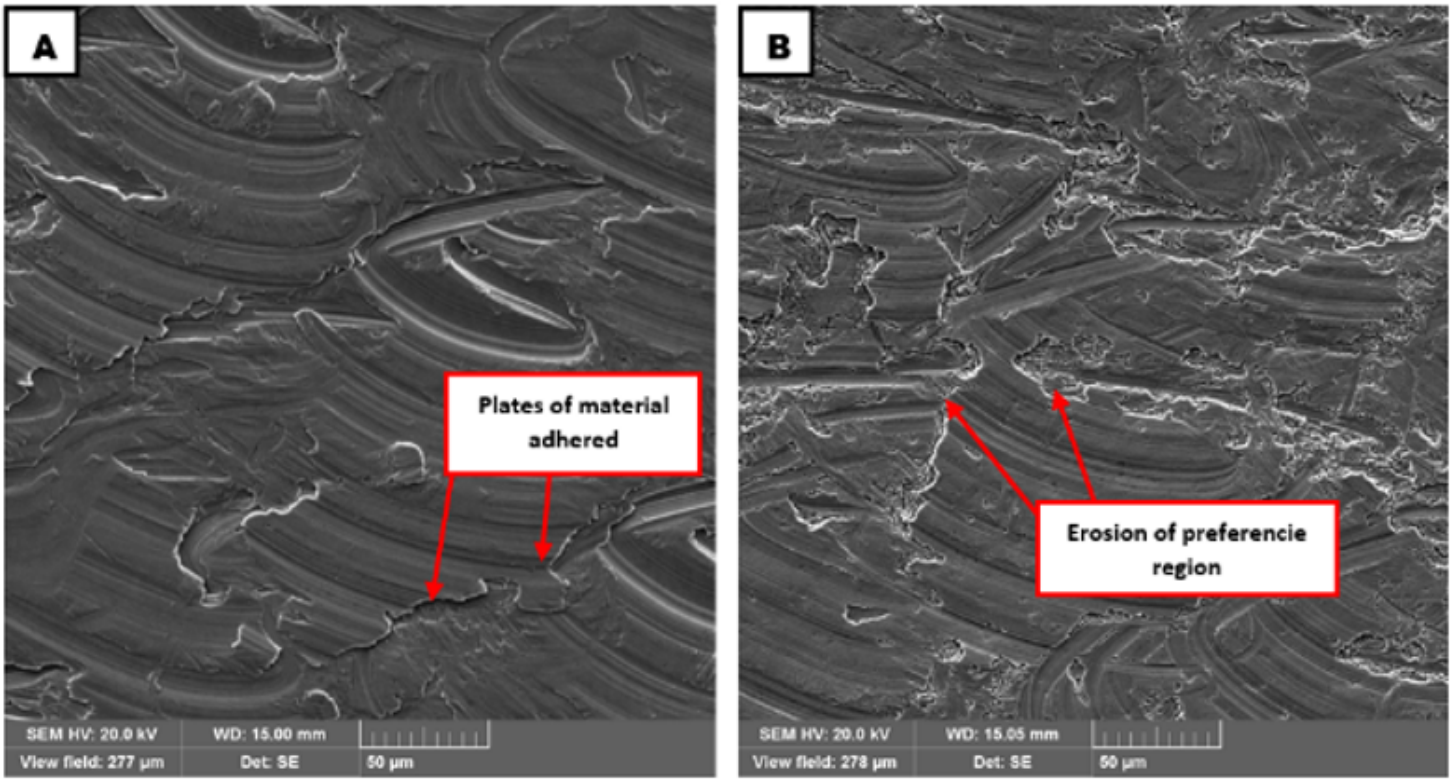

Figure 5

Surface aspect for sample 4N, (A) without cavitation (B) after 6 hours of test

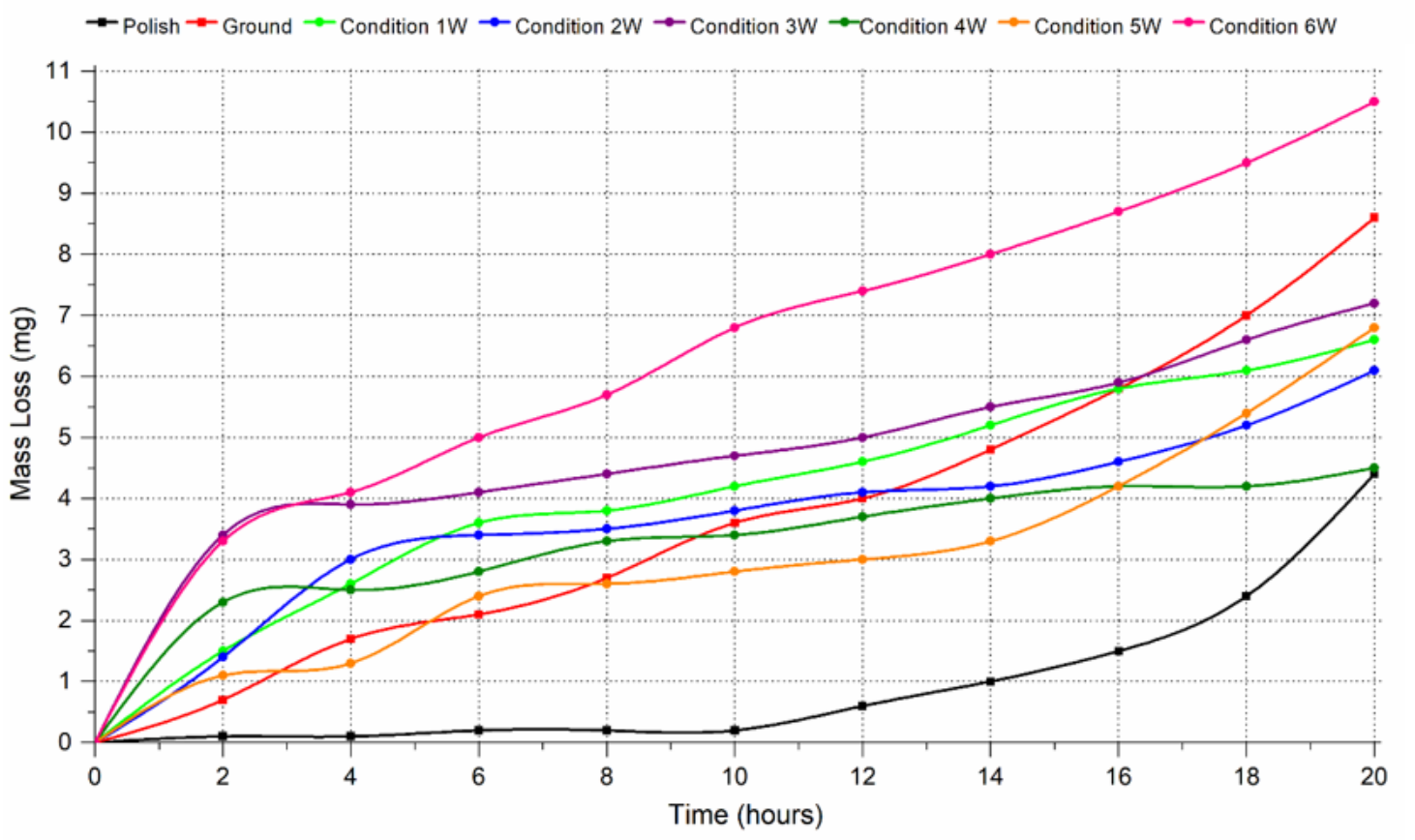

Figure 6

Accumulated mass loss – worn tools

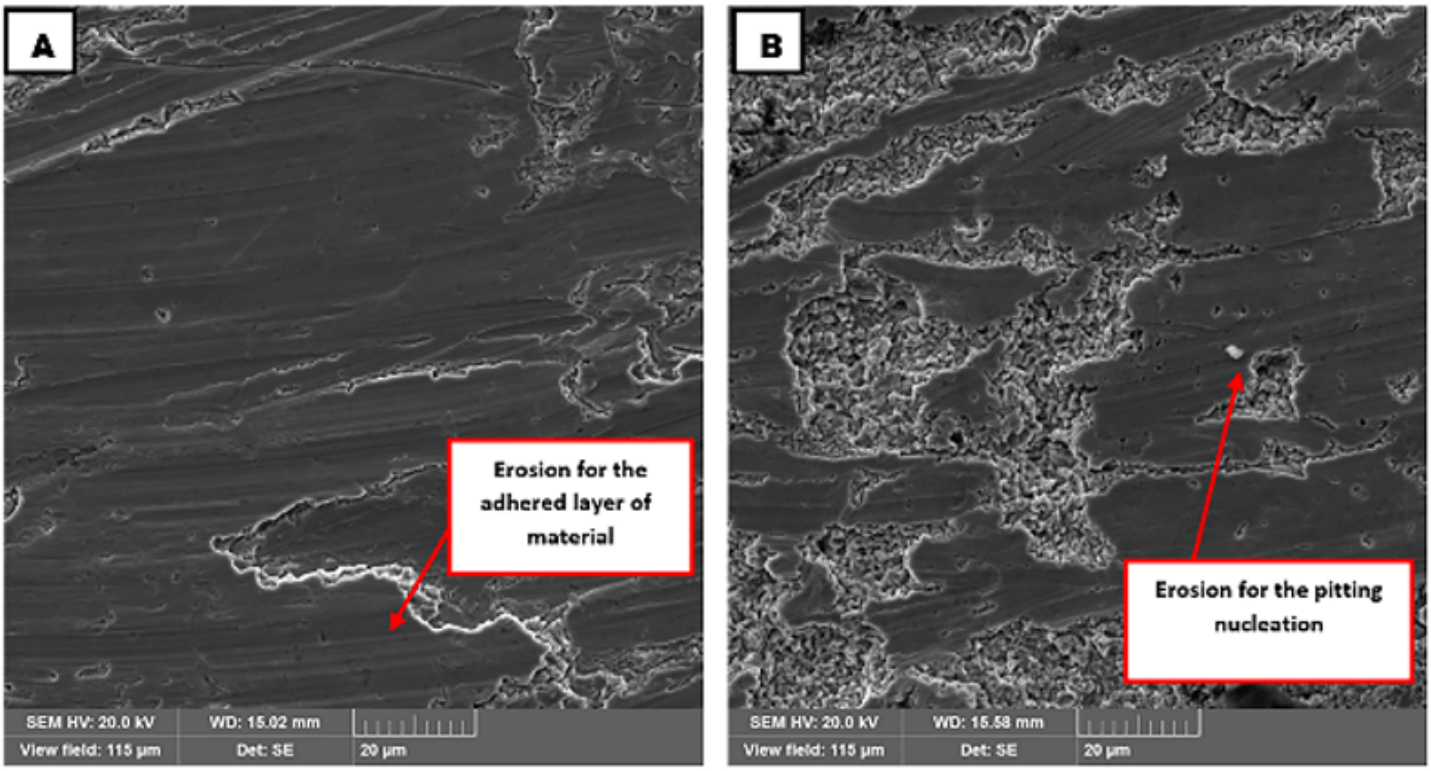

Figure 7

Surface aspect of the sample 4W, (A) 6 hours (B) 20 hours of test

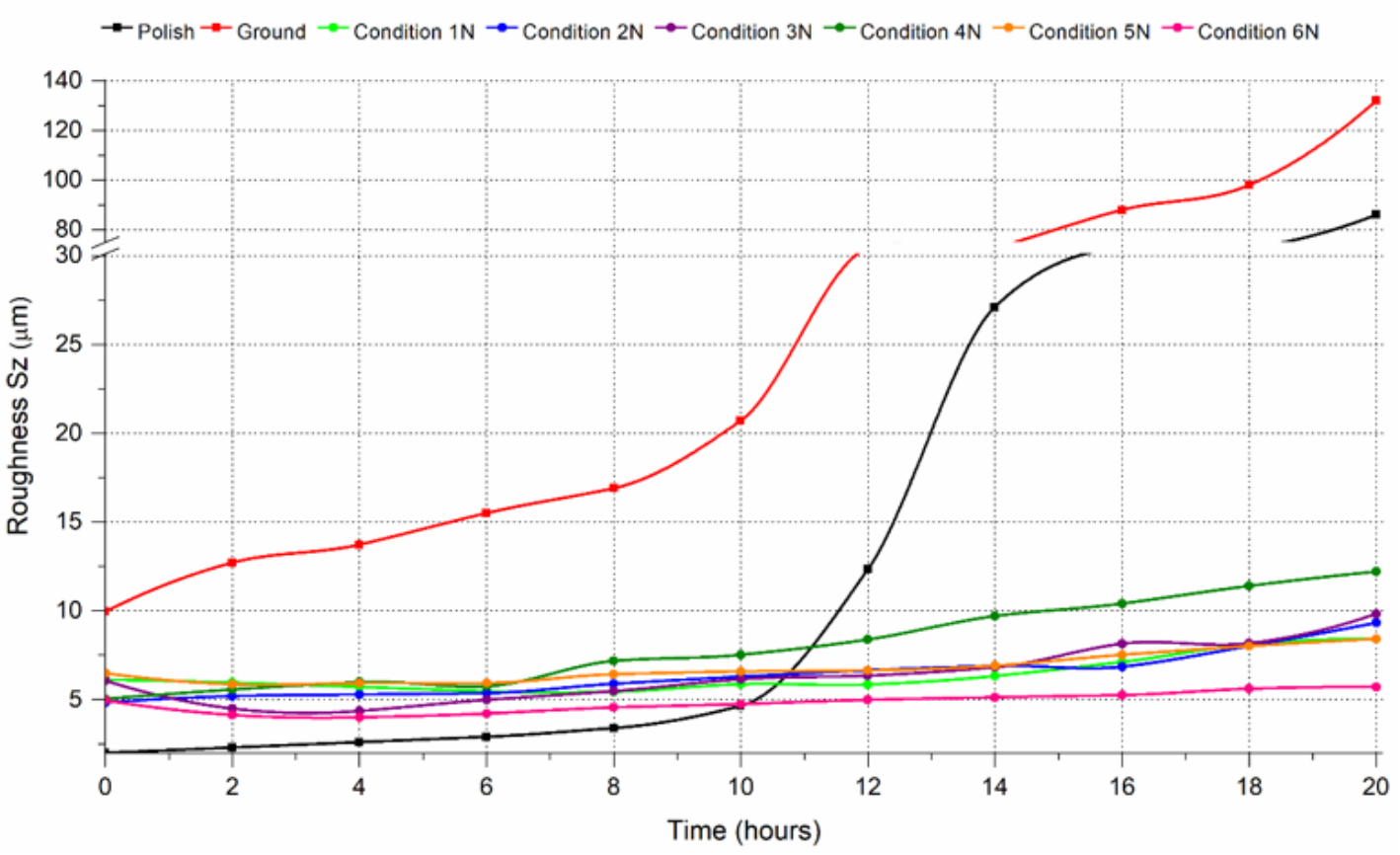

Figure 8

Roughness evolution curve for new tool machined samples

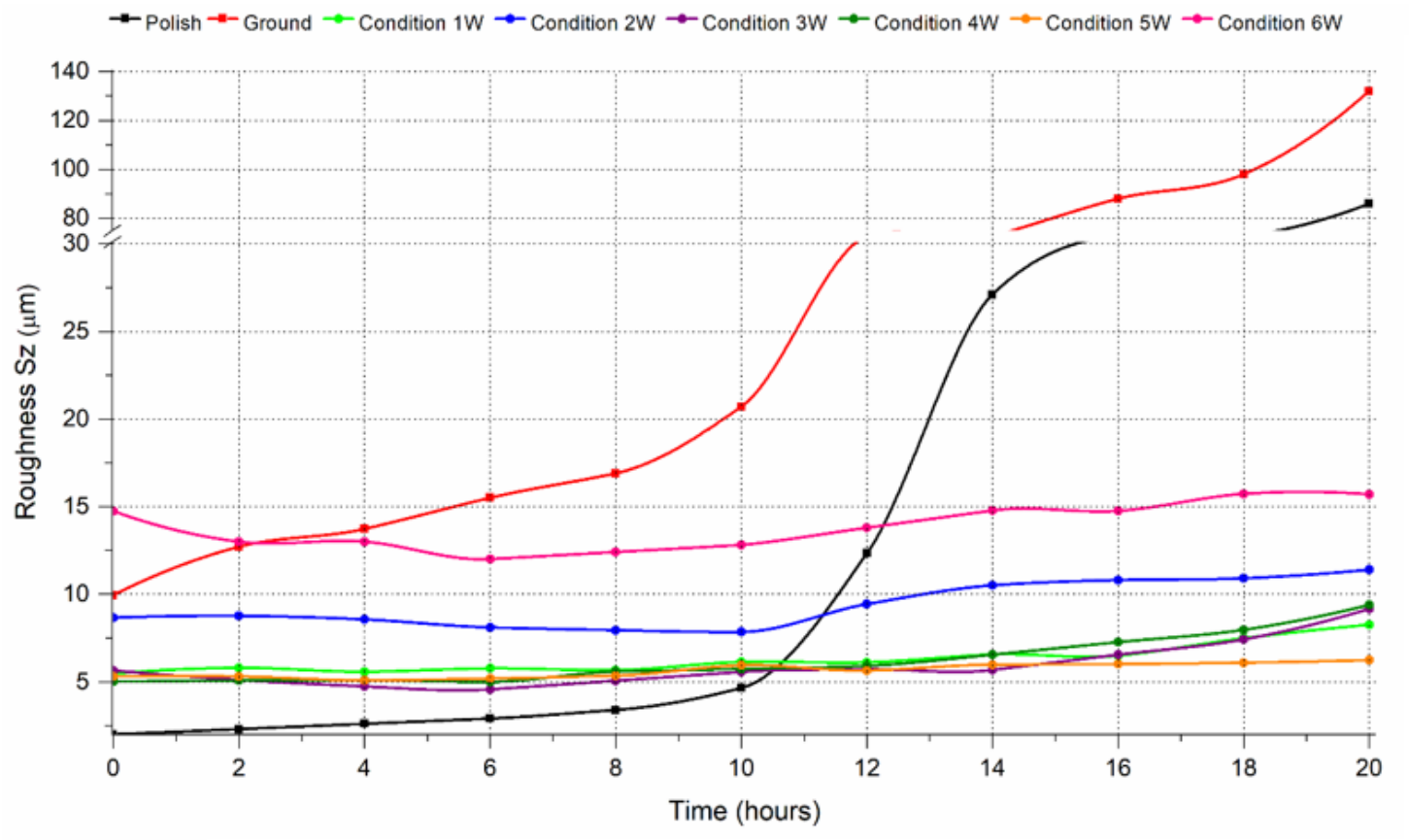

Figure 9

Roughness evolution curve for worn tool machined samples

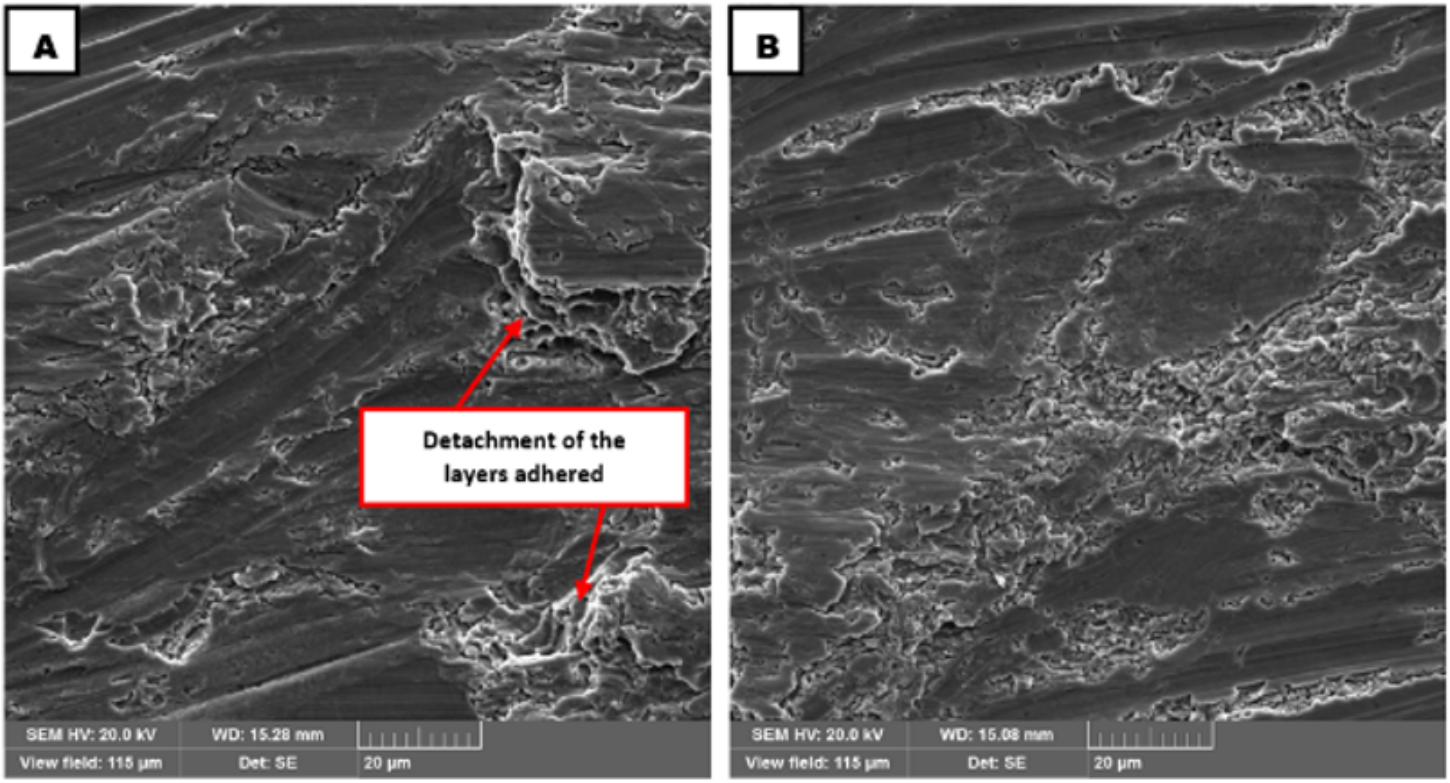

Figure 10

Topographic aspect of 6W sample (A) 6 hours and (B) 10 hours of test

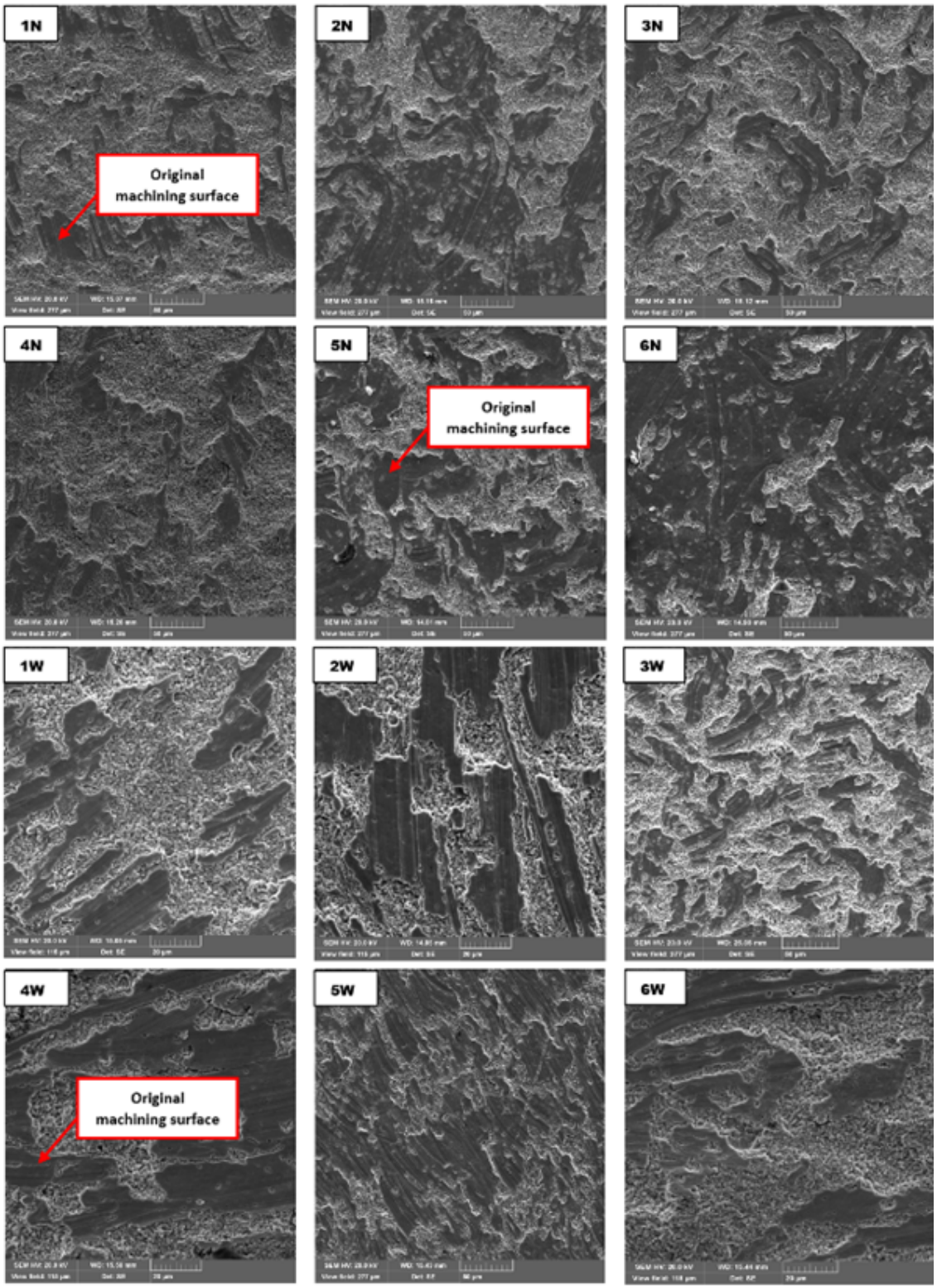

Figure 11

Topographic aspects for machined samples after 20 hours of test. The dark gray color in the photographs represents the original machined surface

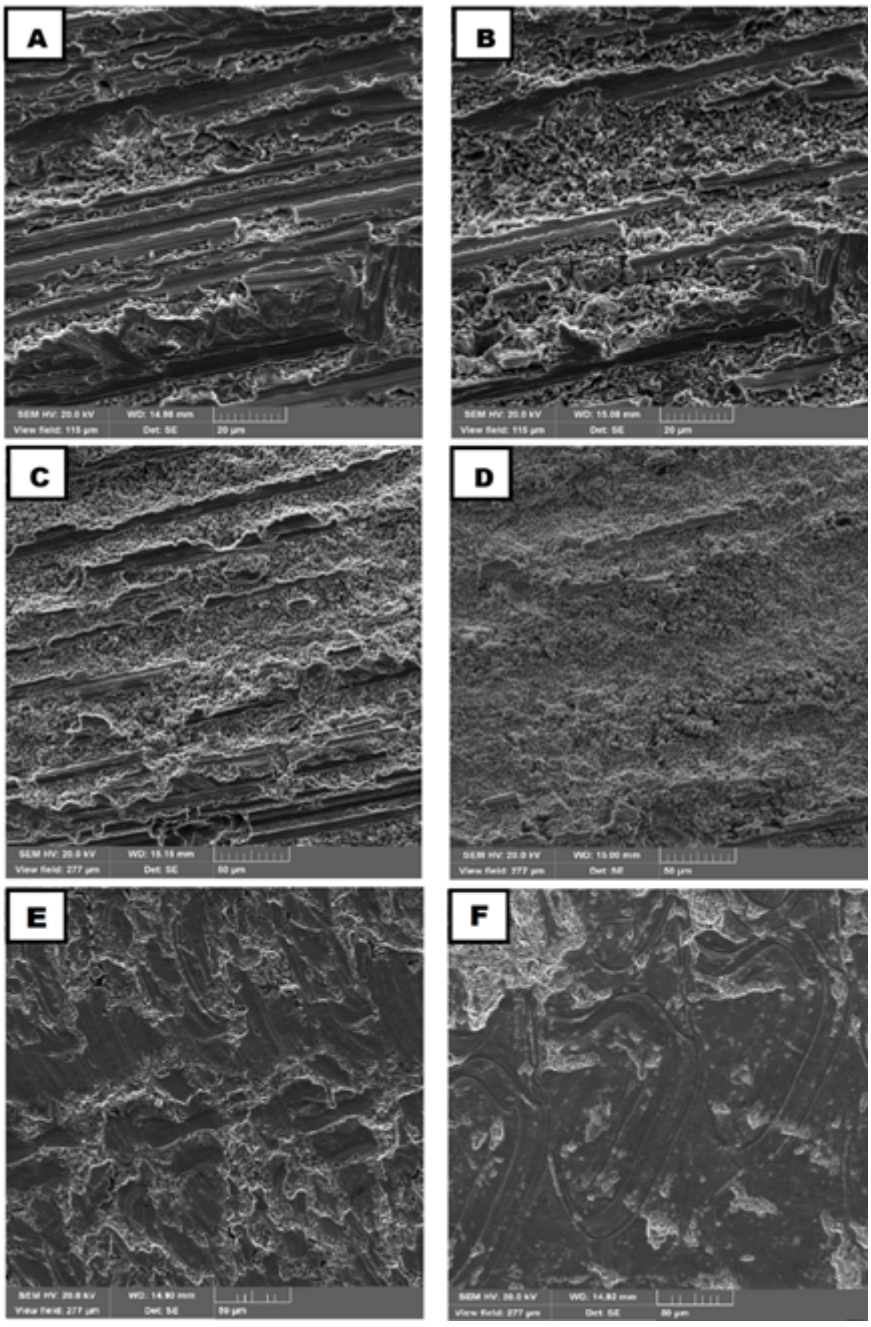

Figure 12

Surface appearance of the ground sample with (A) 6 hours (B) 10 hours (C) 14 hours, (D) 20 hours of test, (E) 14 hours machined surface by interchangeable insert tool and (F) 14 hours machined surface by interchangeable head cutter. The dark gray color in the photographs represents the original ground our machined surface

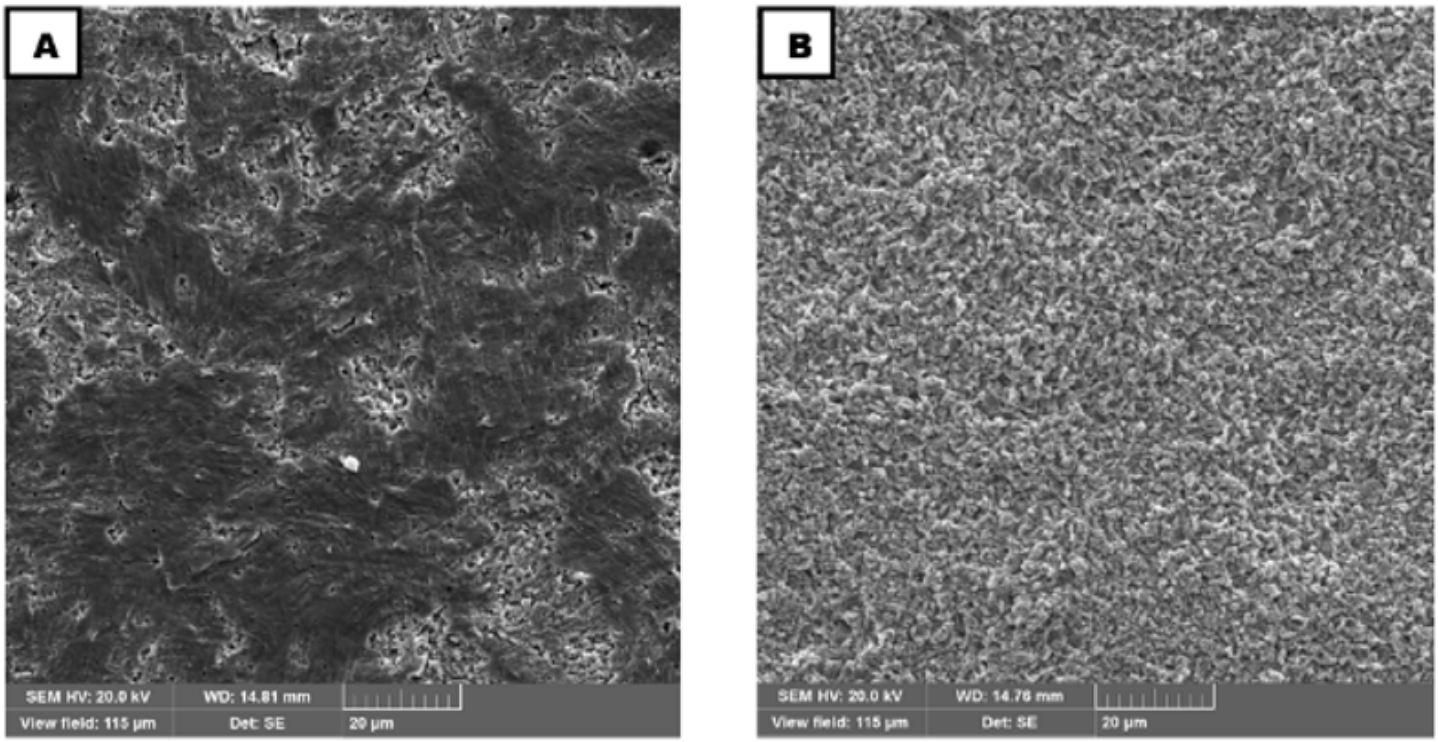

Figure 13

Surface appearance of the polished sample (A) 10 hours e (B) 20 hours of test. The dark gray color in photograph (A) represents the original polished surface

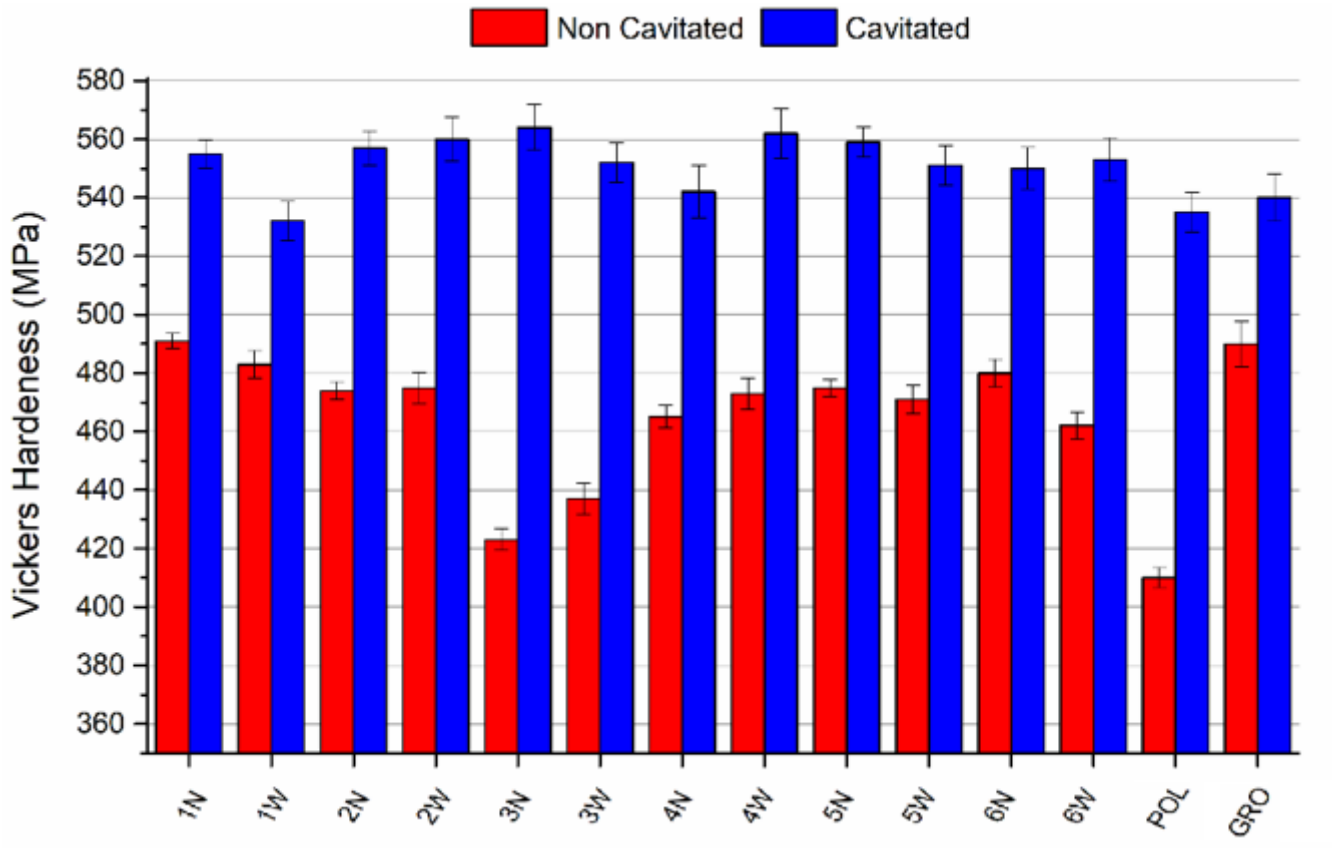

Figure 14

Average hardness of samples tested before and after cavitation test

Supplementary Files

This is a list of supplementary files associated with this preprint. Click to download.

- Highlights.docx